Indian Head Division
Naval Surface Warfare Center
Indian Head, MD 20640-5035

IHCR 06-94
10 February 2006

SCALING OF WATER FLOWS AND OBSTACLE DISPLACEMENTS IN SHALLOW UNDERWATER EXPLOSION FIELD TESTS

By William W. McDonald
NDM Solutions, Subcontractor to Advanced Technology & Research, Corp

For Indian Head Division, Naval Surface Warfare Center
Explosive Effects Branch

Approved for public release; distribution is unlimited.

REPORT DOCUMENTATION PAGE

Form Approved
OMB No. 0704-0188

The public reporting burden for this collection of information is estimated to average 1 hour per response, including the time for reviewing instructions, searching existing data sources, gathering and maintaining the data needed, and completing and reviewing the collection of information. Send comments regarding the burden estimate or any other aspect of this collection of information, including suggestion for reducing this burden, to Department of Defense, Washington Headquarters Services, Directorate for Information Operations and Reports (0704-0188), 1215 Jefferson Davis Highway, Suite 1204, Arlington, VA 22202-4302. Respondents should be aware that notwithstanding any other provision of law, no person shall be subject to any penalty for failing to comply with a collection of information if it does not display a currently valid OMB control number.
PLEASE DO NOT RETURN YOUR FORM TO THE ABOVE ADDRESS.

1. REPORT DATE (DD-MM-YYYY)
10 February 2006

2. REPORT TYPE

3. DATES COVERED (From - To)

4. TITLE AND SUBTITLE
SCALING OF WATER FLOWS AND OBSTACLE DISPLACEMENTS IN SHALLOW UNDERWATER EXPLOSION FIELD TESTS

5a. CONTRACT NUMBER
N00174-04-D-0012/004

5b. GRANT NUMBER

5c. PROGRAM ELEMENT NUMBER

6. AUTHOR(S)
William W. McDonald

5d. PROJECT NUMBER

5e. TASK NUMBER

5f. WORK UNIT NUMBER

7. PERFORMING ORGANIZATIONS NAME(S) AND ADDRESS(ES)
NDM Solutions in support of
Advanced Technology & Research
Spring Pointe Executive Center
15210 Dino Drive
Burtonsville, MD 20866-1712

8. PERFORMING ORGANIZATION REPORT NUMBER

9. SPONSORING/MONITORING AGENCY NAME(S) AND ADDRESS(ES)
Indian Head Division
Naval Surface Warfare Center
Indian Head, MD 20640-5035

10. SPONSOR/MONITOR'S ACRONYM(S)

11. SPONSOR/MONITOR'S REPORT NUMBER(S)
IHCR 06-94

12a. DISTRIBUTION/AVAILABILITY STATEMENT
Approved for public release; distribution is unlimited.

13. SUPPLEMENTARY NOTES

14. ABSTRACT

This work develops a theory for scaling fluid and underwater obstacle motion caused by shallow explosive charges. The motivation is to be able to replicate full-scale test results in subscale experiments despite the fact that gravity remains the same in both tests. The scaling theory is based on the incompressible Euler equations and results for fluid motion are verified through computational example. The applicability of this scaling to obstacle motion is demonstrated by comparing full and subscale obstacle displacement data.

15. SUBJECT TERMS
Obstacle motion
Explosive scaling
Shallow water testing

16. SECURITY CLASSIFICATION OF:			17. LIMITATION OF ABSTRACT	18. NUMBER OF PAGES	19a. NAME OF RESPONSIBLE PERSON
a. REPORT	b. ABSTRACT	c. THIS PAGE			Susan Simpson
U	U	U	SAR	39	19b. TELEPHONE NUMBER (Include area code) (301) 744-4284

This page intentionally left blank.

FOREWORD

The work presented in this report was performed under subcontract ATR-05-S-4164-004 between the author (NDM Solutions) and the Advanced Technology and Research Corporation in support of contract N00174-04-D-0012/0004 with the Naval Surface Warfare Center/Indian Head Division (NSWC/IHD), Indian Head, MD. Dr. Andrew Wardlaw of NSWC/IHD was the task monitor. The author is grateful to Dr. Wardlaw and also to Dr. William Szymczak of the Naval Research Laboratory (ONR) for making calculations using the Gemini and BUB2DS codes that were essential to this effort. Dr. Wardlaw also provided editorial comments that were incorporated in the report. The task is part of a larger effort to evaluate the effectiveness of general-purpose bombs in clearing surf zone obstacles. ONR sponsors are Dr. Thomas Swean and Mr. Brian Almquist.

Amos Dare
Manager, Explosives Effects Branch

Approved by:

Kevin Gessner
Acting Head, Component Technology Division

Released by:

William Yeckley
Acting Head, Energetic Technology Department

This page intentionally left blank.

Contents

Introduction 2
Scaling of Conservation Equations for Incompressible Inviscid Flows 3
Initial and Boundary Conditions 6
Application to Explosion Bubbles 7
Application to Shallow Small-Scale Explosions in The Field 9
Scaling of Obstacle Displacements 19
Experimental Tests of The Shallow Explosion Scaling Theory 21
Conclusions and Recommendations 26
References 27

Figures

1. Tetrahedron and Hedgehog Obstacles 2
2. Full-Scale Run Configuration and Cavity Width/Time Curves for Mk 82 Bomb (Blue) and 7.3-Gram Charge (Red) 12
3. Full-Scale Run Configuration and Cavity Width/Time Curves for Mk 84 Bomb (Blue) and 28-Gram Charge (Red) 12
4. Mk 84 Bomb (Left) and 28-Gram Charge (Right) Development Sequences at Approximately Similar Times 14
5. Radial and Vertical Components of Flow Velocity for Mk 84 Bomb (Blue) and 28-Gram Charge (Red) 15
6. Cavity Widths Comparison - All Charges at Depth Geometrically Similar to Full-Scale Depth 16
7. Frames Showing 1/12-Scale Bubble Developing Upward and Downward Jets After Full-Scale Bubble Has Vented 16
8. Cavity Widths Comparison - Model Charges at Depth of 4.2 Inches to Ensure Venting 17
9. Radial and Vertical Components of Flow Velocity for Mk 84 Bomb (Blue) in 12-ft of Water and 32-gm (Black) and 36-gm (Red) Comp B Charges at 4.2 in. 18
10. Comparison of 7.3-Gram Test Radial Displacements with Scaled Full- Scale Mean (Solid) and $\pm 2\sigma$ Standard Deviation (Dashed) Curves. Colors Denote Different Shots. Diamonds and Squares Denote Toward and Away Orientations. 23
11. Angular Displacements in 7.3-Gram Tests. Colors Denote Different Shots. Diamonds and Squares Denote Toward and Away Orientations. 23
12. Radial Displacements in 28-Gram Tests. Colors Denote Different Shots. Diamonds and Squares Denote Toward and Away Orientations. 25
13. Angular Displacements in 28-Gram Tests. Colors Denote Different Shots. Diamonds and Squares Denote Toward and Away Orientations. 25

Tables

1. Various Possibilities for Exact Scaling of Incompressible Inviscid Flows 6
2. Scale Factors Expressed in terms of Charge Weights 9

This page intentionally left blank.

Scaling of Water Flows and Obstacle Displacements in Shallow Underwater Explosion Field Tests

William W. McDonald, NDM Solutions

in Support of

Advanced Technology & Research, Corp.
Springpointe Executive Center
15210 Dino Drive
Burtonsville, MD 20866-1172
301-989-2499
Fax-301-989-8000

Contract N00174-04-D-0012/004

December 2005

Introduction

The following study is an attempt to better understand the problem of scaling water flows caused by shallow explosive charges in field experiments and, in particular, the motions of objects in the water that are swept along by the flows. The motivation is to be able to use relatively inexpensive small-scale tests to obtain the same information produced by expensive full-scale tests.

The Navy is currently interested in using general-purpose bombs to clear obstacles that have been submerged in shallow water by adversaries to impede landing craft. Obstacles of particular interest are steel constructions know as tetrahedrons and hedgehogs (illustrated in Figure 1). Current research has determined that such obstacles are moved by an explosion primarily as a result of drag forces created by the water flow, although the shock wave also plays a minor role for close-in obstacles. U.S. efforts to study the motions of obstacles using small-scale explosive tests have been underway since 1999.

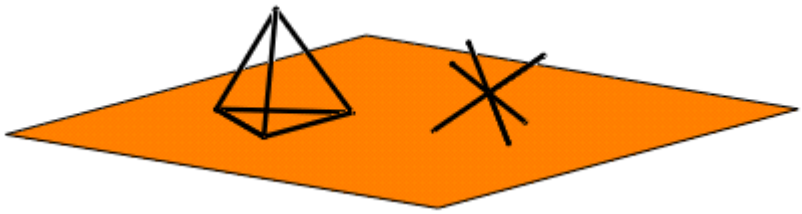

Figure 1. Tetrahedron and Hedgehog Obstacles

Quite obviously, the Navy's interest in scaling the flow of water has a long history. Rigorous research on scaling the water flows of underwater explosions began during World War II and continued for the next several decades. Snay[1] produced a very readable and comprehensive account of this work that addressed many topics and specifically addressed the scaling of underwater explosion shock wave and bubble phenomena. He showed that, while the shock wave can be scaled in small-scale field tests, the scaling of bubble-induced flow phenomena has always required special equipment, such as centrifuges and vacuum tanks, and has never been accurately accomplished in the field. In this report we examine the problem of scaling bubble effects in the field and suggest a way by which this can be achieved for the obstacle clearance problem. Our approach is to seek out the conditions under which the basic equations governing the flow phenomena are invariant under changes of scale.

Scaling of Conservation Equations for Incompressible Inviscid Flows

We examine the requirements for scaling by first considering the conservation equations for incompressible inviscid flows. Szymczak[2] has shown that explosion bubble phenomena near the free surface can be accurately modeled by satisfying, over the fluid and gas domains, the mass and momentum conservation equations

$$\rho_t + \nabla\cdot(\rho\mathbf{u}) = 0 \tag{1}$$

$$(\rho\mathbf{u})_t + \nabla\cdot(\rho\mathbf{u}\mathbf{u}) = -\rho g\mathbf{k} - \nabla p\ , \tag{2}$$

subject to various constraints and justifiable assumptions regarding the bubble gas, cavitated regions, and the ambient atmosphere. Other important contributors are acknowledged in Reference 3. In the water, the flow is treated as incompressible and the equations simplify to

$$\nabla\cdot\mathbf{u} = 0 \tag{3}$$

$$\rho\mathbf{u}_t + \rho\nabla\cdot(\mathbf{u}\mathbf{u}) = -\rho g\mathbf{k} - \nabla p\ , \tag{4}$$

with pressure and velocity initial conditions, and boundary conditions applied at the water surface and bottom, at the gas-water surface that forms the explosion bubble, and at the boundaries of cavitation regions, when they exist. In axisymmetric cylindrical coordinates, Equations (3) and (4) are

$$\frac{1}{r}\frac{\partial ru}{\partial r} + \frac{\partial w}{\partial z} = 0 \quad \text{(Continuity)} \tag{5}$$

$$\rho\left[\frac{\partial u}{\partial t} + u\frac{\partial u}{\partial r} + w\frac{\partial u}{\partial z}\right] = -\frac{\partial p}{\partial r} \quad \text{(Horizontal Momentum)} \tag{6}$$

$$\rho\left[\frac{\partial w}{\partial t} + u\frac{\partial w}{\partial r} + w\frac{\partial w}{\partial z}\right] = \rho g - \frac{\partial p}{\partial z} \quad \text{(Vertical Momentum)}, \tag{7}$$

where u and w are the velocity components in the radial and vertical directions.

By introducing horizontal and vertical characteristic lengths L_r and L_z, respectively, and a characteristic time T, we can put the left sides of Equations (5), (6), and (7) into dimensionless forms. Upon substitution of the quantities $u = \frac{L_r}{T}u^*$, $w = \frac{L_z}{T}w^*$, $r = L_r r^*$, $z = L_z z^*$, and $t = Tt^*$, where starred terms are dimensionless, we obtain

$$\frac{1}{L_r r^*}\frac{\partial\left(L_r r^* \frac{L_r}{T}u^*\right)}{\partial\left(L_r r^*\right)} + \frac{\partial\left(\frac{L_z}{T}w^*\right)}{\partial\left(L_z z^*\right)} = 0 \tag{8}$$

$$\rho\left[\frac{\partial\left(\frac{L_r}{T}u^*\right)}{\partial\left(Tt^*\right)}+\frac{L_r}{T}u^*\frac{\partial\left(\frac{L_r}{T}u^*\right)}{\partial\left(L_r r^*\right)}+\frac{L_z}{T}w^*\frac{\partial\left(\frac{L_r}{T}u^*\right)}{\partial\left(L_z z^*\right)}\right]=-\frac{\partial p}{\partial\left(L_r r^*\right)} \tag{9}$$

$$\rho\left[\frac{\partial\left(\frac{L_z}{T}w^*\right)}{\partial\left(Tt^*\right)}+\frac{L_r}{T}u^*\frac{\partial\left(\frac{L_z}{T}w^*\right)}{\partial\left(L_r r^*\right)}+\frac{L_z}{T}w^*\frac{\partial\left(\frac{L_z}{T}w^*\right)}{\partial\left(L_z z^*\right)}\right]=\rho g-\frac{\partial p}{\partial\left(L_z z^*\right)}. \tag{10}$$

Rearrangement and some cancellations yield the dimensionless equations

$$\frac{1}{r^*}\frac{\partial r^* u^*}{\partial r^*}+\frac{\partial w^*}{\partial z^*}=0 \tag{11}$$

$$\frac{\partial u^*}{\partial t^*}+u^*\frac{\partial u^*}{\partial r^*}+w^*\frac{\partial u^*}{\partial z^*}=-\frac{T^2}{L_r}\frac{1}{\rho}\frac{\partial p}{\partial r} \tag{12}$$

$$\frac{\partial w^*}{\partial t^*}+u^*\frac{\partial w^*}{\partial r^*}+w^*\frac{\partial w^*}{\partial z^*}=\frac{T^2}{L_z}g_0 g'-\frac{T^2}{L_z}\frac{1}{\rho}\frac{\partial p}{\partial z}. \tag{13}$$

It is noted that these results require a single characteristic time rather than different characteristic times for each direction. In Equation (13), we have replaced g by $g_0 g'$, where we have chosen the acceleration of gravity at sea level, g_0, as our characteristic gravity, and g' is a dimensionless gravity. For reasons that will later become clear, we write this as g' rather than g^*. We can also call g' the gravity scale factor.

The partial derivatives on the right hand sides of Equations (12) and (13) can be made dimensionless by transforming to r^* and z^*, and introducing the characteristic pressure $P = L_r L_z \big/ \rho T^2$, so that $p = Pp^*$. In this manner we can express the conservation equations as

$$\frac{1}{r^*}\frac{\partial r^* u^*}{\partial r^*}+\frac{\partial w^*}{\partial z^*}=0 \tag{14}$$

$$\frac{\partial u^*}{\partial t^*}+u^*\frac{\partial u^*}{\partial r^*}+w^*\frac{\partial u^*}{\partial z^*}=-N_r^{-1}\frac{\partial p^*}{\partial r^*} \tag{15}$$

$$\frac{\partial w^*}{\partial t^*}+u^*\frac{\partial w^*}{\partial r^*}+w^*\frac{\partial w^*}{\partial z^*}=F^{-1}-N_z^{-1}\frac{\partial p^*}{\partial z^*}, \tag{16}$$

where the quantities N_r, N_z, and F are given by

$$N_r = \frac{\rho L_r^2}{T^2 P}, \quad N_z = \frac{\rho L_z^2}{T^2 P}, \quad \text{and} \quad F = \frac{L_z}{g_0 g' T^2} \quad . \tag{17}$$

N_r, N_z, and F are respectively known as the Newton numbers in the r and z directions and the Froude number. The Newton numbers are associated with dynamic inertial effects and the Froude number is associated with gravitational effects.

The model and full-scale tests will be governed by the same dimensionless equations if the Newton and Froude numbers appropriate for the model-scale, which we shall denote by primes, equal those appropriate for the full scale. That is, if $N_r' = N_r$, $N_z' = N_z$, and $F' = F$, it may be said that the model and full-scale equations then possess dynamic similarity, in the respective directions, and also gravitational similarity. The scaling conditions are thus

$$\frac{1}{\rho'}\frac{T'^2 P'}{L_r'^2} = \frac{1}{\rho}\frac{T^2 P}{L_r^2} \quad \text{or} \quad \left(\frac{T'}{T}\right)^2 \frac{P'}{P} = \left(\frac{L_r'}{L_r}\right)^2 \frac{\rho'}{\rho} \tag{18}$$

$$\frac{1}{\rho'}\frac{T'^2 P'}{L_z'^2} = \frac{1}{\rho}\frac{T^2 P}{L_z^2} \quad \text{or} \quad \left(\frac{T'}{T}\right)^2 \frac{P'}{P} = \frac{\rho'}{\rho}\left(\frac{L_z'}{L_z}\right)^2 \tag{19}$$

$$\frac{T'^2}{L_z'} g' = \frac{T^2}{L_z} \quad \text{or} \quad \left(\frac{T'}{T}\right)^2 g' = \frac{L_z'}{L_z} \quad . \tag{20}$$

The time, pressure, length, and density scale factors appear on the right hand sides of Equations (18), (19), and (20). Defining the symbols $\tau \equiv T'/T$, $\varphi = \frac{P'}{P}$, $\lambda_r = \frac{L_r'}{L_r}$, $\lambda_z = \frac{L_z'}{L_z}$, and $\pi = \frac{\rho'}{\rho}$, to identify these scale factors, respectively, we can rewrite the scaling conditions as

$$\tau^2 \varphi = \pi \lambda_r^2 \tag{21}$$

$$\tau^2 \varphi = \pi \lambda_z^2 \tag{22}$$

$$\tau^2 g' = \lambda_z \tag{23}$$

Equations (21) and (23) call for geometric similarity, i.e., $\lambda_r = \lambda_z = \lambda$, which, in turn, requires equality of the Newton numbers $N_r = N_z = N$.

The remaining scaling conditions are

$$\tau^2 \varphi = \pi \lambda^2 \tag{24}$$

$$\tau^2 g' = \lambda \ . \tag{25}$$

Satisfying Equations (24) and (25) in different ways leads to different types of equivalent experimental designs, all of which yield the same flow information. All of these may be referred to as Froude and Newton scaling. The possibilities of interest are listed in Table I. These include high gravity and low pressure scaling, which have been successfully used in the past to scale explosion bubble phenomena, and also high density and the mixed type scaling where the density and pressure of the model both differ from those of the full-scale test. High gravity scaling requires the use of a centrifuge, while low pressure scaling (sometimes referred to as vacuum tank scaling) requires an enclosed tank from which the atmosphere can be partially evacuated. All scale factor values in Table I, other than unity and the pressure scale factor φ in the case of the mixed design (E5), are expressed as functions of the length scale factor, which at this point is arbitrary. Under E5, φ is also arbitrary.

Table 1. Various Possibilities for Exact Scaling of Incompressible Inviscid Flows

Experimental Design	Length λ	Time τ	Pressure φ	Density π	Gravity g'	Scaling Description
E1	1	1	1	1	1	Full-Scale
E2	λ	λ	1	1	$1/\lambda$	High Gravity
E3	λ	$\sqrt{\lambda}$	λ	1	1	Low Pressure
E4	λ	$\sqrt{\lambda}$	1	$1/\lambda$	1	High Density
E5	λ	$\sqrt{\lambda}$	φ	φ/λ	1	Mixed Type

Initial and Boundary Conditions

Equality of the model and full-scale dimensionless conservation equations is not alone sufficient for achieving flow similarity. In addition, the dimensionless initial and boundary conditions for the model and full-scale flows must also be identical. The initial condition requires similarity of the velocity field $\mathbf{v}(r,z,t)$ at similar initial times, t_0 and t_0'. We, thus, require

$$\frac{T}{L}\mathbf{v}(\frac{r}{L},\frac{z}{L},\frac{t_0}{T}) = \mathbf{v}^*(r^*,z^*,t_0{}^*) = \frac{T'}{L'}\mathbf{v}'(\frac{r'}{L'},\frac{z'}{L'},\frac{t_0'}{T'}), \tag{26}$$

or equivalently,

$$\mathbf{v}(r,z,t_0) = \frac{\tau}{\lambda}\mathbf{v}'(r',z',t_0'), \quad r' = \lambda r, \quad z' = \lambda z, \quad t_0' = \tau t_0, \tag{27}$$

for all points in the fluid domain.

The boundaries of the model must, of course, be geometrically similar to the boundaries of the full-scale test. The numerical conditions that must be satisfied at the boundaries are described by Szymczak in Reference 2 (p.5). The pressures must satisfy Neumann conditions on "wall" boundaries and Dirichlet conditions on nonliquid surfaces, such as those of gas bubbles and the air-water interface. Szymczak states that the Neumann condition, or value of $\partial p/\partial \mathbf{n}$ on the "wall" boundary, implies that the normal component of the flow velocity is zero, i.e.,$\mathbf{v}\cdot\mathbf{n}$, where $\mathbf{n}$ is the unit normal to the boundary at the point (r, z). The dimensionless condition $\mathbf{v}^*\cdot\mathbf{n}$ then follows immediately. Reference 2 also describes a viscoplastic model suitable for saturated sand boundaries that we will not address as this review is motivational rather than comprehensive.

The Dirichlet conditions require continuity of the pressure on the free surfaces. At the air-water interface the dimensionless pressure in the water p^* must equal the dimensionless atmospheric pressure p_A^*. It then follows that

$$\frac{p'_A}{P'} = \frac{p'}{P'} = p^* = \frac{p}{P} = \frac{p_A}{P}$$

or

$$p'_A = \frac{P'}{P} p_A = \varphi\, p_A \ . \tag{28}$$

That is, the model atmospheric pressure must equal the full-scale atmospheric pressure multiplied by the pressure scale factor at all times *t*. In a closely related fashion, the adiabatically changing explosion bubble pressure in the model and full-scale tests, $p'_B(t')$ and $p_B(t)$ respectively, must satisfy

$$p'_B(t') = \varphi\, p_B(t) \tag{29}$$

at all similar times *t* and $t' = \tau t$, including the initial times t_0 and t'_0. It also follows that scaling restricts model cavitation bubble pressures. If p_C is the cavitation (vapor) pressure in the full-scale test (assumed constant), the model cavitation pressure must be

$$p'_C = \varphi\, p_C \ . \tag{30}$$

Because p_B is related to the detonation pressure of the explosive and p_C is the vapor pressure of the fluid medium, it is very difficult to satisfy Equations (29) and (30) when designs with a reduced value of φ are used, such as E3 and E5. As pointed out by Snay (Reference 1, p.50), because of these difficulties "any model test represents an approximation" and "the problem of scaling requires a thorough understanding of the physics of the phenomena" to judge which effects should be strictly reproduced in the model experiment and which can be ignored. The literature on vacuum tank scaling contains details of the techniques used to control many of these effects.[4]

Application to Explosion Bubbles

When the conservation equations are applied to underwater explosion bubbles, the characteristic length attributed by Cole to G.I. Taylor, that relates *L* to "the total energy available after emission of the shock wave" (Cole[5], p 291), is often used:

$$L = \left(\frac{E}{\rho g_0 g'} \right)^{1/4} . \tag{31}$$

Today, *E* is called the bubble energy. If we use Equation (31) to define an energy scale factor ε, we get

$$\varepsilon = \frac{E'}{E} = \frac{\rho'}{\rho} \left(\frac{L'}{L} \right)^4 g' = \pi\, \lambda^4 g' \ . \tag{32}$$

This shows that ε is proportional to λ^4 for testing design E3 ($g' = 1$, $\pi = 1$), and to λ^3 for methods E2 ($g' = 1/\lambda$, $\pi = 1$), E4 ($g' = 1$, $\pi = 1/\lambda$), and E5 ($g' = 1$, $\pi = \varphi/\lambda$).

In their review of spherical bubble theory, Szymczak and Solomon[3] (referencing Friedman[6]) stated that the bubble energy *E* is usually assumed to be proportional to the explosive charge weight *W* (mass). The constant of proportionality *Q* was shown to be

$$Q = \frac{4\pi}{3} J_\infty^3 , \tag{33}$$

where J_∞ is related to the usual bubble radius coefficient J by the equation

$$J = J_\infty \left[\frac{1-\alpha^{3(1-\gamma)}}{1-\alpha^{-3\gamma}} \right]^{-1/3} . \tag{34}$$

Here $\alpha = A_{\max} / A_{\min}$ is the ratio of the maximum and minimum bubble radii, and γ is the ratio of specific heats of the bubble gas, which is assumed to behave adiabatically. Szymczak and Solomon pointed out that *J* is not a constant because α is a function of the charge depth (or hydrostatic pressure), but that J_∞ may be regarded as a constant characteristic of the explosive. While this has been known (e.g., see References 1 and 7), explosives handbooks and test reports have usually tabulated *J* values instead of J_∞ values. Thus, the energy scale factor can be expressed as

$$\varepsilon = \frac{E'}{E} = \left(\frac{J'_\infty}{J_\infty} \right)^3 \frac{W'}{W} , \tag{35}$$

and we may substitute J'/J for J'_∞ / J_∞ when both the full-scale and model charges are subjected to the same hydrostatic pressures. Otherwise, an appropriate correction should be made based, for example, on the theory of Szymczak and Solomon.

By combining Equation (35) with Equation (32), the various scale factors of Table I can be expressed in terms of the charge weights. These are shown in Table II. The scale factors of Table II apply to all flow quantities of the model test and all of its boundary and initial conditions. In the case of E3, it should be noted that, because the length scale factor is proportional to the fourth root of the charge weight ratio, it cannot be used to size the model charge. λ only pertains to the model charge when the cube root applies and when the same explosive is used in both the model and full-scale tests.

Table 2. Scale Factors Expressed in terms of Charge Weights

	Length λ	**Time** τ	**Pressure** φ	**Density** π	**Gravity** g'
E1	1	1	1	1	1
E2	$\left[\left(\frac{J'_\infty}{J_\infty}\right)^3 \frac{W'}{W}\right]^{1/3}$	$\left[\left(\frac{J'_\infty}{J_\infty}\right)^3 \frac{W'}{W}\right]^{1/3}$	1	1	$\left[\left(\frac{J'_\infty}{J_\infty}\right)^3 \frac{W'}{W}\right]^{-1/3}$
E3	$\left[\left(\frac{J'_\infty}{J_\infty}\right)^3 \frac{W'}{W}\right]^{1/4}$	$\left[\left(\frac{J'_\infty}{J_\infty}\right)^3 \frac{W'}{W}\right]^{1/8}$	$\left[\left(\frac{J'_\infty}{J_\infty}\right)^3 \frac{W'}{W}\right]^{1/4}$	1	1
E4	$\left[\left(\frac{J'_\infty}{J_\infty}\right)^3 \frac{W'}{W}\right]^{1/3}$	$\left[\left(\frac{J'_\infty}{J_\infty}\right)^3 \frac{W'}{W}\right]^{1/6}$	1	$\left[\left(\frac{J'_\infty}{J_\infty}\right)^3 \frac{W'}{W}\right]^{-1/3}$	1
E5	$\left[\left(\frac{J'_\infty}{J_\infty}\right)^3 \frac{W'}{W}\right]^{1/3}$	$\left[\left(\frac{J'_\infty}{J_\infty}\right)^3 \frac{W'}{W}\right]^{1/6}$	φ	$\varphi\left[\left(\frac{J'_\infty}{J_\infty}\right)^3 \frac{W'}{W}\right]^{-1/3}$	1

Predictions of any full-scale quantity, such as the horizontal velocity component u induced by an explosion at the point (r, z) at time t, can be obtained from the measurement of the quantity at the homologous point (r', z') and time t' in the small-scale test by applying the appropriate scaling relationship. The scaling relationships can be obtained by expressing both the full-scale and model-scale quantities in dimensionless forms and equating them as was done for Equation (26). This follows because both comply with the dimensionless conservation equations. Thus, for the u velocity component we have

$$\frac{T}{L}u(\frac{r}{L},\frac{z}{L},\frac{t}{T}) = u^*(r^*,z^*,t^*) = \frac{T'}{L'}u'(\frac{r'}{L'},\frac{z'}{L'},\frac{t'}{T'}) . \tag{36}$$

Hence, we express the full-scale quantity u in terms of the small-scale measurement u' as

$$u(r,z,t) = \frac{\tau}{\lambda}u'(r',z',t'), \quad r' = \lambda r, \quad z' = \lambda z, \quad t' = \tau t . \tag{37}$$

Similar expressions can be developed for any other quantities.

Application to Shallow Small-Scale Explosions in the Field

Small-scale field experiments conducted, for example, in ponds, lakes, and filled quarries are problematic when approached using traditional bubble scaling methods. Table II shows that Hopkinson scaling, or the use of cube root length and time scale factors, does not apply to bubble phenomena unless the gravity scale factor is raised, which cannot be accomplished in the field. High density scaling could be used in the field if a suitable inviscid higher density fluid could be found. Low pressure scaling could be used in the field if a suitable structure could be built over the body of water to allow reduction of the atmospheric pressure. The Mixed Type scaling could be used to ease the pressure load on the structure, but would again require the involvement of special fluids.

Of the several methods considered above, the low pressure method is the closest to satisfying the requirements for exact scaling in the field because it involves the same fluid used in the full-scale experiment and is conducted under normal gravity. In fact, all of the requirements for low pressure scaling can be met in the field except some of those related to the scaling of the pressures.

In the field, the principal scaling difficulty is caused by our inability to control the static atmospheric pressure. The hydrostatic pressure, due to the weight of the water, is reduced by the geometric scale factor and is, therefore, properly scaled. Hence, the forces that distort the bubble shape are properly scaled when the water boundaries and bubble geometry are properly scaled. Scaling fails in field experiments primarily because the normal atmospheric pressure suppresses the growth of the bubble and produces bubbles that are too small. Indeed, shallow field explosions that vent under full-scale conditions often fail to vent in small-scale field experiments. The reduced atmospheric pressure, required by low pressure scaling, allows the bubble to grow larger than it would grow under the normal atmospheric pressure. Hence, under low pressure scaling the reduction of the atmospheric pressure is simply a way of achieving the correct bubble size. This suggests that if the size of the bubble could be properly controlled, the rest of the flow would behave in a manner similar to the full-scale flow.

These considerations have led to the realization that low pressure scaling rules, with the exception of the pressure rule, might apply in the field if the bubble can be grown to the proper size. The three methods available for growing the bubble are (1) to vary the energy released in the explosion, (2) to change the charge depth, and (3) some combination of both. Varying the charge weight would change the amount of explosive gas in the bubble and distort the bubble collapse and the flow during later bubble cycles. Thus, method (1) is attractive for modeling bubbles that vent, but would appear to be less attractive for modeling nonventing bubbles. Changing the model charge depth to adjust the bubble size presents the obvious problem of changing the flow geometry. The consequences, however, may be insignificant when the change in depth is small relative to the overall bubble size. In particular, method (2) may also be effective for scaling venting explosions in shallow water.

When venting occurs, the pressure in the bubble cavity and the atmospheric pressure rapidly equalize. Indeed, the assumption that the bubble pressure changes to the air pressure instantaneously upon venting is employed in the BUB2DS and BUB3DS codes (Reference 3, p2-4). Thus, any additional bubble gas associated with method (1) above would simply be exhausted upon venting and would not appear to complicate the subsequent flow. For shallow shots, the bubble usually vents before its internal pressure reaches the vapor pressure; hence, it is also unlikely that cavitation would be a complicating factor.

The relationships between scale factors and charge weight listed in Table II cannot be expected to be valid for flows induced by venting bubbles. The bubble energy, or energy available to drive the flow, can no longer be assumed to be proportional to the charge weight. This is because differing venting conditions result in differing fractions of the explosion energy being exhausted to the atmosphere. Instead, the relationships between scale factors and charge weights for venting bubbles must be found by numerical simulations of the flows.

In collaboration with Szymczak at NRL and Wardlaw at IHDNSWC, both methods (1) and (2) were investigated computationally with favorable results. Using the BUB2DS incompressible code, Szymczak simulated the behavior of a vertical Mk 82 bomb with its nose touching the bottom in six feet of water for both full-scale and 1/12th-scale field conditions.[8] In each case, he assumed an initial cylindrical bubble with a volume equal to the volume of the actual charge. For the 1/12th-scale test, he used a 7.3 grams Comp B charge that was sized using the low pressure scaling conditions with the appropriate J values. The length to diameter ratio of the initial bubble for the model charge was taken to be 2.3. The depth of the model charge was decreased until the model cavity width versus time curve matched the scaled down full-scale curve. Scaling of the full-scale curve was done by multiplying the cavity width by the 1/12 length scale factor and the time by the $1/\sqrt{12}$ time scale factor, as required under low pressure scaling rules. The center depth of the model charge was 2.4 inches instead of the 3.3 inches needed for geometric similarity. Cavity widths were measured at cells just above the rigid bottom. Figure 2 shows the configuration and indicates that the two cavity width versus time curves matched extremely well.

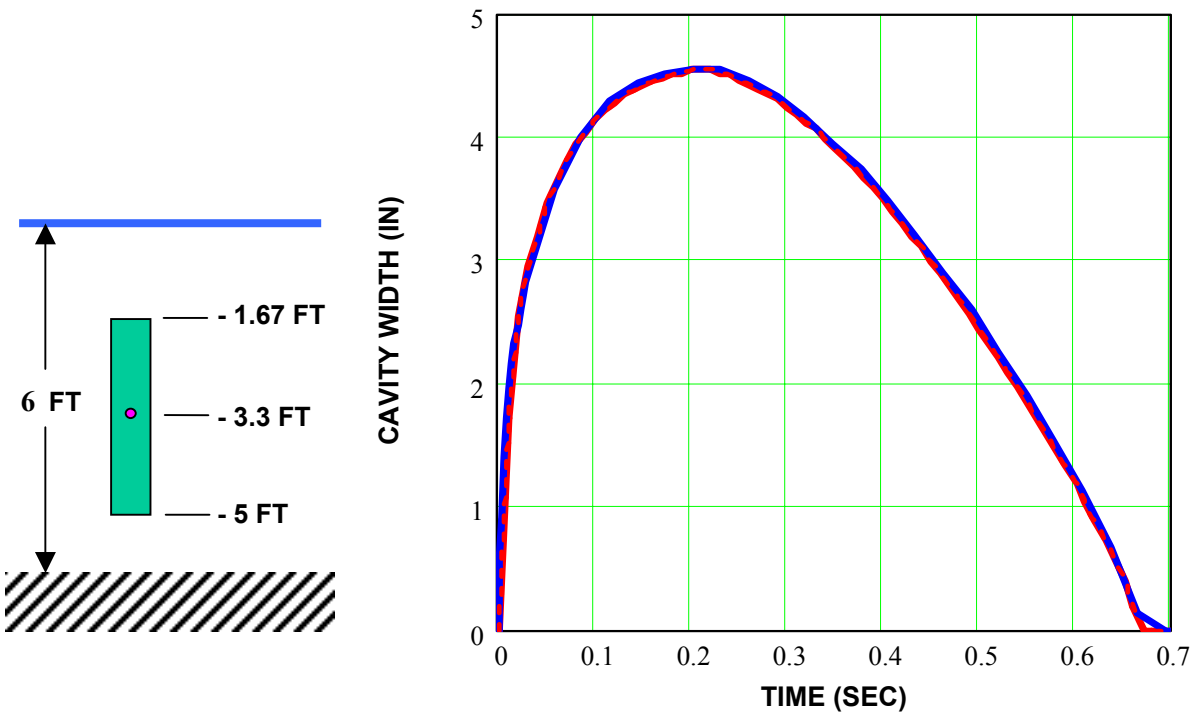

Figure 2. Full-Scale Run Configuration and Cavity Width/Time Curves for Mk 82 Bomb (Blue) and 7.3-Gram Charge (Red)

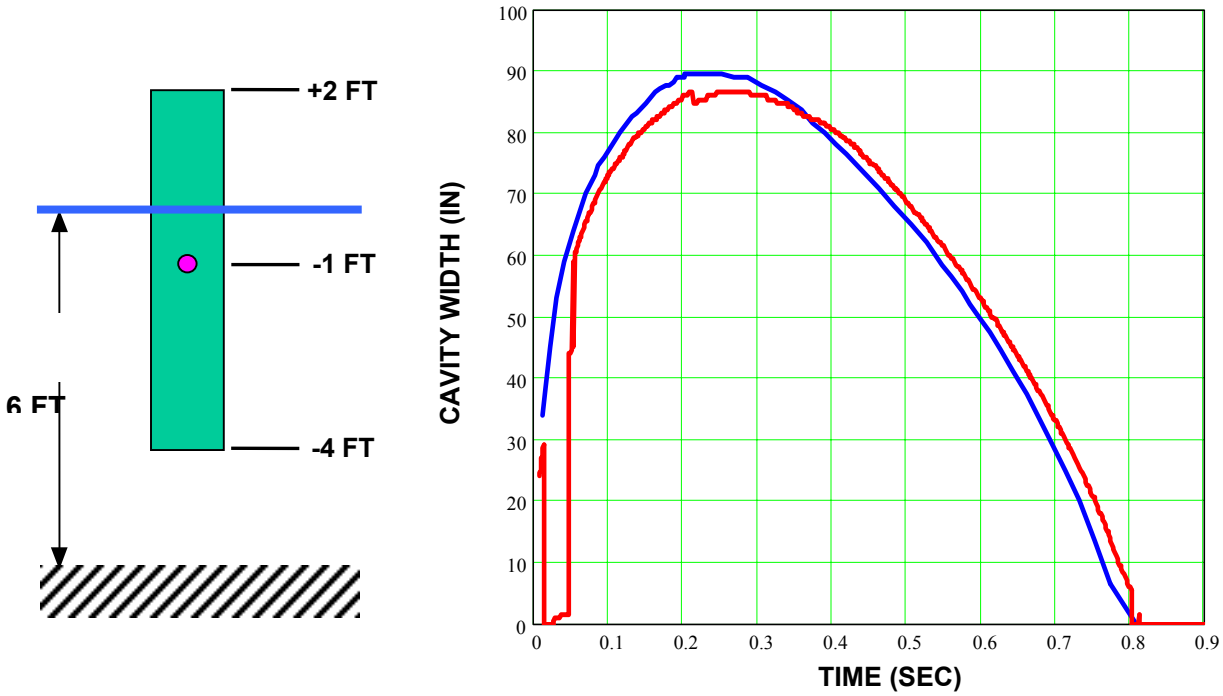

Figure 3. Full-Scale Run Configuration and Cavity Width/Time Curves for Mk 84 Bomb (Blue) and 28-Gram Charge (Red)

Wardlaw[9] modeled at both full-scale and 1/12th-scale the flow produced by a vertical Mk 84 bomb with its nose touching the bottom in six feet of water, as depicted in Figure 3. Because in this case, approximately one third of the bomb extends out of the water, the events were first modeled using Wardlaw's Gemini compressible hydrocode.∗ When the explosive burn was completed, Wardlaw linked the results to the BUB2DS incompressible code, using the velocity field produced by Gemini, and continued the calculations to completion. The model charge was geometrically similar to the full-scale charge (assumed to be cylindrical) in the vertical direction, but its diameter was reduced to achieve the desired explosive weight. This method was chosen to keep the same fractions of the explosive charge above and below the water surface for all runs. The charge weight was varied from that required by low pressure scaling (36 gms) until the cavity width versus time curve of the model matched that of the scaled down full-scale calculation. The best match, which is shown in Figure 3, occurred for a charge weight of 28 grams. That the quality of the match is somewhat below that shown in Figure 2 is thought to be due to the fact that the calculation was more complex. To obtain an accurate simulation of the explosive burn and to get the shock wave well beyond the bubble, the Gemini run had to be rezoned three times. The difficulty of controlling the rezoning times may have introduced differences. There was also a discontinuity in the linkage of the codes and a non-physical pressure pulse caused by the incompressibility of the BUB2DS code.[9]

The finding that the charge size needed to grow the bubble was less than that predicted by low pressure scaling, rather than more, deserves comment. It is thought that this is because the diameter of the model charge was smaller than that of the scaled down full-scale charge. Because the charge length was kept geometrically similar, a diameter smaller than the geometrically similar diameter had to be used to achieve charge weights on the order of those required by $1/4^{th}$ root low pressure scaling. The smaller charge diameter and the higher pressure at the surface resulted in a more efficient coupling of the energy of the model charge to the water. Because the full-scale charge diameter was larger, the explosion gases could more easily escape the cavity. The complete explanation is complicated, however, because the stronger shock wave of the full-scale charge relative to the model charge (shock wave phenomena follow cube root scaling rules) would probably result in more spalling at the surface. It is presently unclear whether this would enhance or suppress the growth of the full-scale cavity.

Figure 4 shows selected frames from movies of the computations for the Mk 84 bomb and the 28-gram charge at approximately similar times. The flows appear to be quite similar, although irregularities are evident that may be due to the complications mentioned by Wardlaw and listed above. Radial and vertical components of the flow velocity were recorded at mid-depth stations at several distances from the origin. These are shown in Figure 5. The horizontal velocity components appear be a somewhat better match than the vertical components. Nevertheless, the overall agreement between the model and full-scale flows is again quite good. Moreover, the agreement between the velocity components appears to be best at early times.

∗ Compressible flow equations follow Hopkinson (high gravity) scaling. No attempt was made here to scale the compressible flow. Rather, the hydrocode was simply being used to establish initial conditions for the incompressible flow.

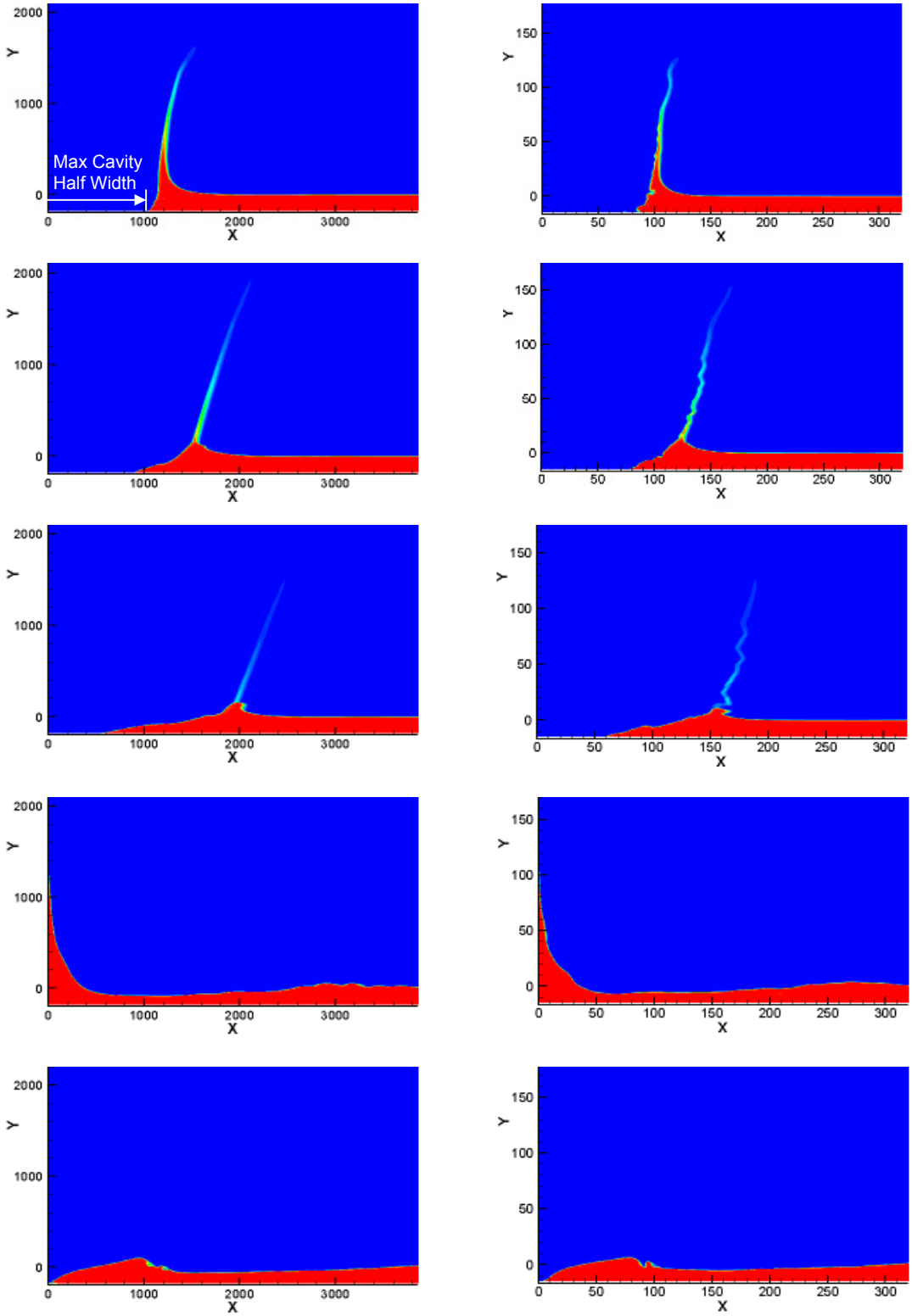

Figure 4. Mk 84 Bomb (Left) and 28-Gram Charge (Right) Development Sequences at Approximately Similar Times

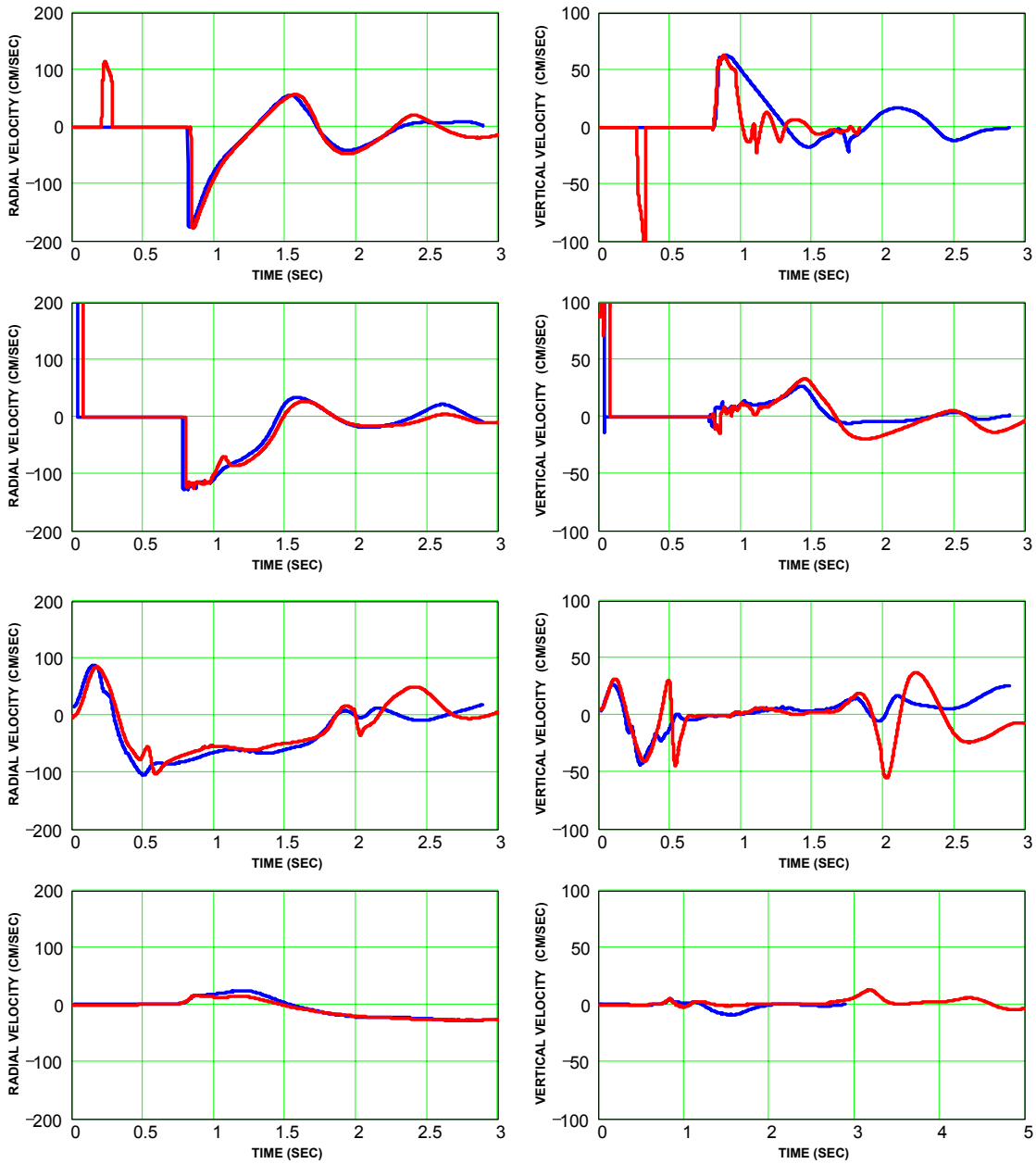

Figure 5. Radial and Vertical Components of Flow Velocity for Mk 84 Bomb (Blue) and 28-Gram Charge (Red)

The calculations suggest that the entire velocity field is matched when the cavity width versus time curves are in agreement, particularly after venting time. When the bubbles have vented and the entire free surface, including the cavity wall, is at atmospheric pressure, the velocity field alone determines the future history of the flow. The fact that the model is at atmospheric pressure, rather than the reduced level prescribed by the low pressure scaling rules, does not affect the flow after venting because the conservation equations depend on the pressure through the gradient only. Hence, it appears that the agreement of the velocity fields following venting guarantees the similarity of the flows.

Figures 6 and 7 show that it is not always possible to match the cavity width history by increasing the model charge weight at the geometrically scaled full-scale charge depth. In this numerical experiment performed by Wardlaw using the BUB2DS code (initialized by Gemini), conditions were similar to that shown in Figure 3 except that the water depth was increased to 12 feet.[10] The Mk 84 bomb was then fully submerged. Cavity width plots for 48 and 42 grams of Comp B, shown in Figure 6, suggested that a smaller charge weight was required to match the scaled down full-scale curve. The charge weight required by the low pressure scaling law was 36 grams. The run at 39 grams, however, showed both (1) that a smaller size charge was needed to be on the scaled full-scale curve and (2) that the bubbles of such smaller charges would not vent. Figure 7 shows the 39-gm bubble developing downward and upward jets at a scaled time after the full-scale bubble had vented. Apparently, the high atmospheric pressure in the model test (relative to that of the low pressure scaling rule) prevented the bubble from opening.

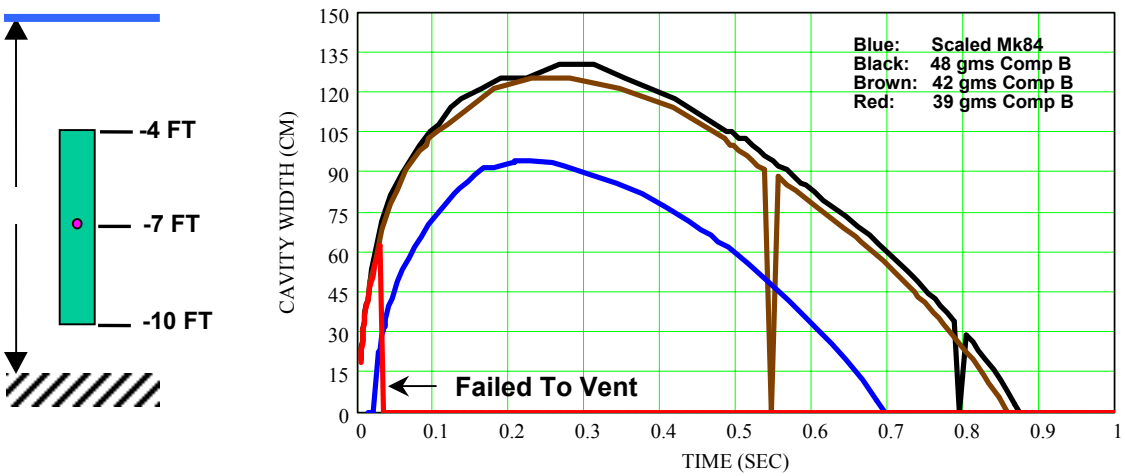

Figure 6. Cavity Widths Comparison - All Charges at Depth Geometrically Similar to Full-Scale Depth

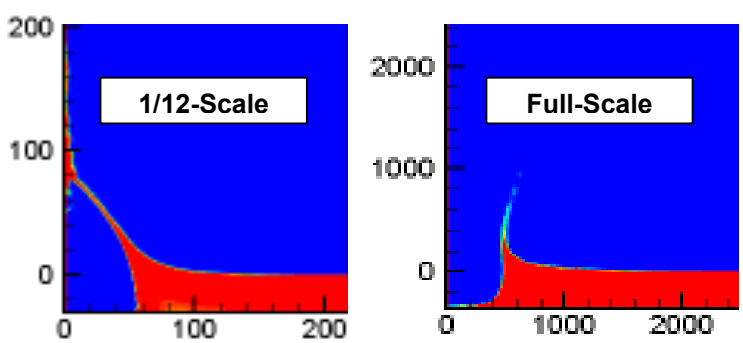

Figure 7. Frames Showing 1/12-Scale Bubble Developing Upward and Downward Jets After Full-Scale Bubble Has Vented

Figure 8 shows that it was possible to match the cavity width versus time curve for the Mk 84 bomb in 12 feet of water by reducing the depth of the model charge.[10] The charge depth was changed from 7 inches to 4.2 inches to obtain a charge depth to maximum bubble radius ratio of 0.2 for the 36-gram charge, which was the value of the ratio in Szymczak's simulation of the Mk 82 bomb in 6 feet of water. A tested empirical rule is that bubbles shallower than a quarter of a maximum bubble radius vent under normal atmospheric pressure; hence, this depth was chosen to ensure venting. The size of the maximum bubble radius was obtained from the empirical bubble equation. The 39-gram charge at depth of 7 inches had a ratio of about one third, and, as seen above, did not vent.

From Figure 8 we see that the cavity width versus time curve of the 32-gram charge was in reasonably good agreement with the scaled full-scale curve. The 36-gram curve is also shown. Figure 9 shows the radial and vertical velocity components at selected horizontal stations for all three runs. The radial components are, perhaps, in better overall agreement than the vertical components. Fine-scale differences between all three computations are apparent in the movies of the flows, and these may be responsible for some of the differences shown in Figure 9. On the whole, the agreement between the model and full-scale velocity components is quite acceptable.

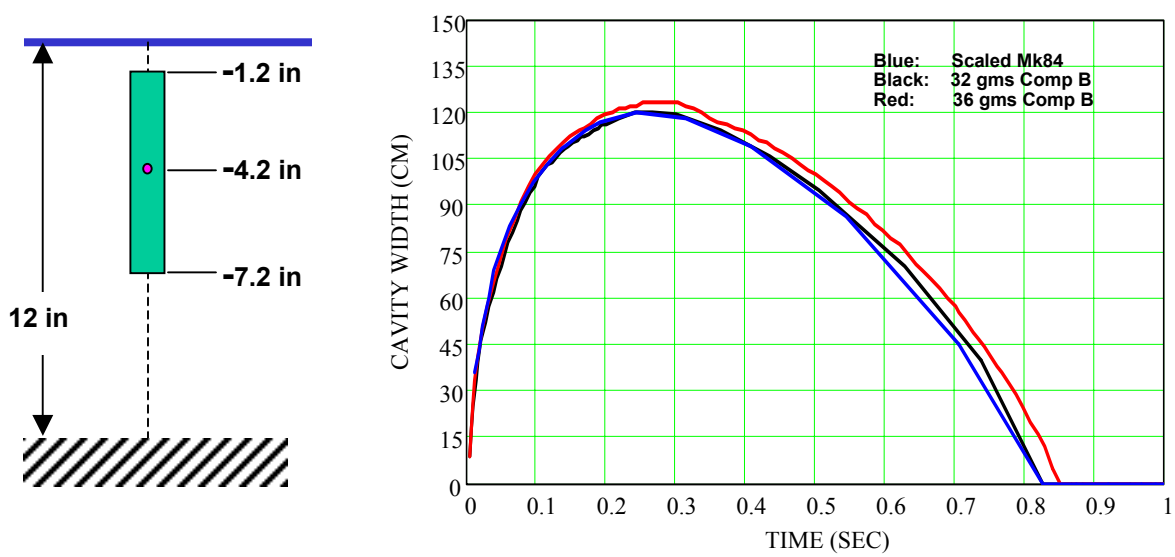

Figure 8. Cavity Widths Comparison - Model Charges at Depth of 4.2 Inches to Ensure Venting

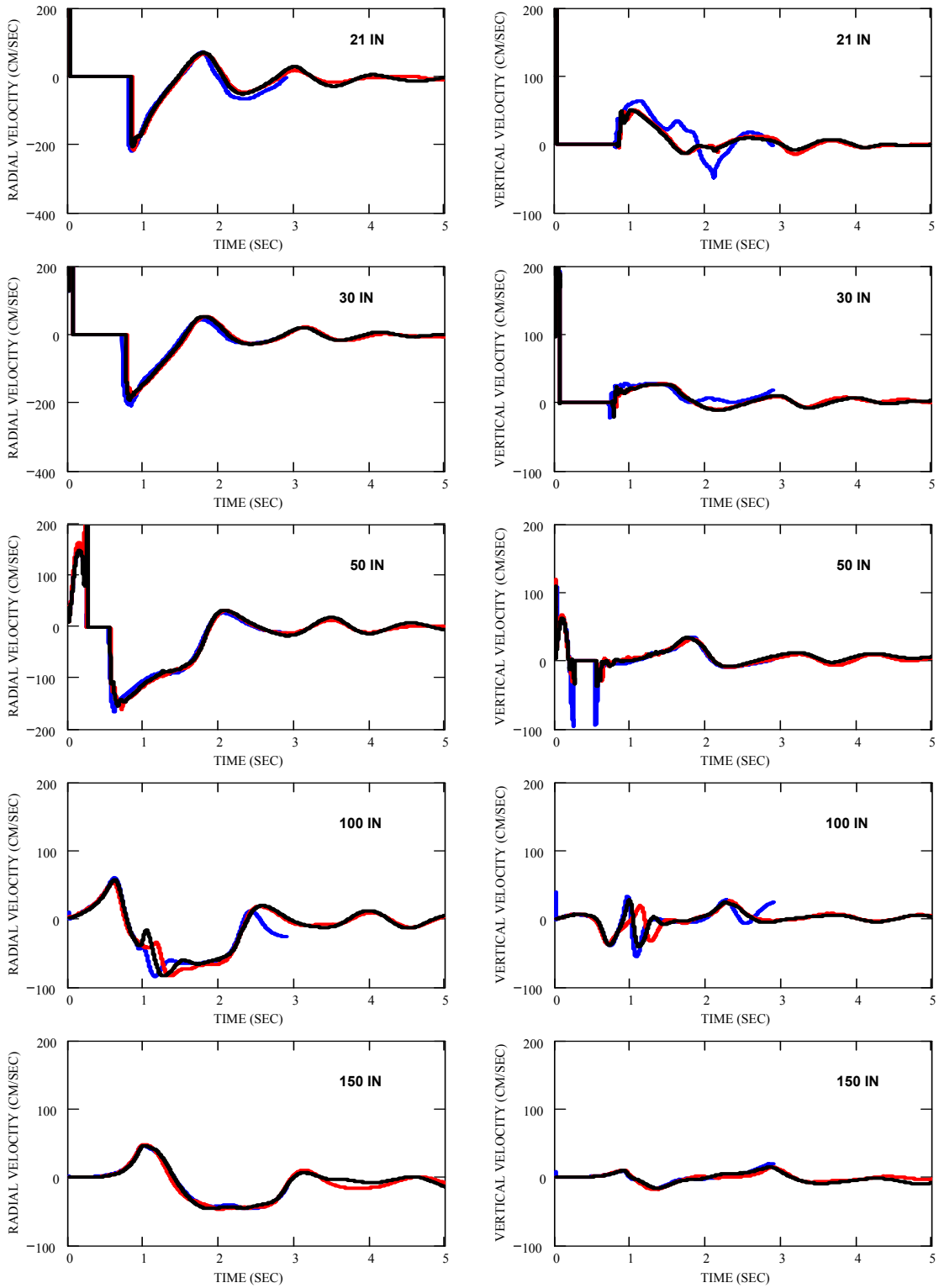

Figure 9. Radial and Vertical Components of Flow Velocity for Mk 84 Bomb (Blue) in 12-ft of Water and 32-gm (Black) and 36-gm (Red) Comp B Charges at 4.2 in.

Scaling of Obstacle Displacements

We now examine whether obstacles placed in the small scale flow field behave in manners that are similar to their behavior under full-scale conditions. We examine first the case of an obstacle that translates without rotation. Computer generated animations of obstacle motions made by Wardlaw (using a rigid body model of the motions of a tetrahedron coupled to Szymczak's BUB2DS incompressible hydrocode that has been started using, as in the case of the Mk 84 bomb, the GEMINI hydrocode) showed that, in some cases, obstacles did not rotate appreciably while being transported by the flow.[11] Generally, however, obstacles do rotate during translation. We will comment at the conclusion of this section on the effects rotations may have on the motion of the obstacle and the issue of scaling.

If the translating obstacle is lifted and translated by the flow, a first approximation of the equations governing the obstacle's motion can be assumed to be

$$(m + m_{A_r})\ddot{r} = \frac{1}{2}\rho C_r a_r (u - \dot{r})^2 \tag{38}$$

in the horizontal direction and

$$(m + m_{A_z})\ddot{z} = \frac{1}{2}\rho C_z a_z (w - \dot{z})^2 - m g_0 g' \tag{39}$$

in the vertical direction. Here, m is the mass of the obstacle, m_{A_r} and m_{A_z} are added masses for flows in the r and z directions, respectively, a_r and a_z are the areas of the obstacle presented to the horizontal and vertical components of the flow, and C_r and C_z are the drag coefficients. Equations (38) and (39) are based, in part, on an analysis performed by Goeller and Ruben,[12] who studied the case of an obstacle that is driven horizontally by the water flow and is resisted by frictional contact with the bottom. They concluded that a "constant drag coefficient appears reasonable; that is, there is little dependence on Reynolds Number." Hence, we shall assume that C_r and C_z are unvarying constants.

The need for added masses in the governing equations is a currently unresolved issue. They are not employed by Wardlaw in his hydrocode-coupled rigid body code because the obstacle mass is being driven by the flow rather than driving it.[11] We shall carry them along, nevertheless, in the event that they prove to be necessary during some phases of the motion.

The obstacle masses and the area presented to the horizontal flow component will vary if the length scale L of the obstacle is changed. We can assume that the variation of the mass of the obstacle with L can be represented as

$$m = \rho_{obs} L^3 f_m. \tag{40}$$

Here ρ_{obs} is the density of obstacle material and $f_m = V/L^3$, is a dimensionless form factor that is independent of scale, where V is the obstacle volume. Similarly, the variation with L of the area presented to the horizontal flow can be written as

$$a_r = L^2 f_{a_r}, \tag{41}$$

where f_{a_r} is a dimensionless horizontal area form factor. In like manner, we write the presented area in the vertical direction as

$$a_z = L^2 f_{a_z} . \tag{42}$$

The added masses of the obstacle are somewhat more involved. Assuming potential flow, Pozrikidis has shown[13] that the kinetic energy K of the fluid for a general motion of a rigid body of volume V can be written as

$$K = \frac{1}{2} \rho V A_{ij} W_i W_j , \tag{43}$$

where $W = (u, v, w, \omega_x, \omega_y, \omega_z)'$ is a vector of translational and rotational velocity components of the rigid body and A_{ij} is the symmetric six-by-six grand added mass matrix. Pozrikidis states that the "value of A depends exclusively upon the instantaneous body shape and orientation and presence of other objects, but is independent of the body's linear or angular velocity or acceleration." The important idea for us is that A depends on body shape, but not its scale. Since we are assuming translational motion in two directions only, A has only three nonzero terms corresponding to the r and z directions and a cross term. Because the volume dimensions are proportional to their associated scale factors, Equation (43) shows that it is possible to represent the virtual masses by the forms

$$m_{A_r} = \rho L^3 f_{m_{A_r}} \tag{44}$$

and

$$m_{A_z} = \rho L^3 f_{m_{A_z}} , \tag{45}$$

where $f_{m_{A_r}}$ and $f_{m_{A_z}}$ are dimensionless form factors that involve elements of the grand added mass matrix.

If we insert Equations (40), (41), (42), (44), and (45) into Equations (38) and (39), along with the expressions $\ddot{r} = \frac{L}{T^2}\ddot{r}^*$, $\ddot{z} = \frac{L}{T^2}\ddot{z}^*$, $\dot{r} = \frac{L}{T}\dot{r}^*$, $\dot{z} = \frac{L}{T}\dot{z}^*$ and, as before, $u = \frac{L}{T}u^*$ and $w = \frac{L}{T}w^*$, in which the starred quantities are dimensionless, we get

$$(\rho_{obs} f_m + \rho f_{m_{A_r}}) L^3 \frac{L}{T^2}\ddot{r}^* = \frac{1}{2}\rho C_r L^2 f_{a_r} (\frac{L}{T}u^* - \frac{L}{T}\dot{r}^*)^2 \tag{46}$$

$$(\rho_{obs} f_m + \rho f_{m_{A_z}}) L^3 \frac{L}{T^2}\ddot{z}^* = \frac{1}{2}\rho C_z L^2 f_{a_z} (\frac{L}{T}w^* - \frac{L}{T}\dot{z}^*)^2 - \rho_{obs} L^3 f_m g_0 g' \tag{47}$$

If we insert $\frac{L}{T^2} = F g_0 g'$ from Equations (17) and rearrange, we obtain

$$\ddot{r}^* = \frac{\frac{1}{2} C_r \rho f_{a_r}}{(\rho_{obs} f_m + \rho f_{m_{A_r}})} (u^* - \dot{r}^*)^2 \tag{48}$$

and

$$\ddot{z}^* = \frac{\frac{1}{2} C_z F \rho f_{a_z} (w^* - \dot{z}^*)^2 - \rho_{obs} f_m}{F(\rho_{obs} f_m + \rho f_{m_{A_z}})} . \tag{49}$$

Equations (48) and (49) show that the displacement equations are invariant under Froude scaling, i.e., when the Froude number F is the same for both model and full-scale tests.

Obstacle rotations will add one to three additional equations of motion, depending upon the initial obstacle symmetries, or lack of symmetries, relative to the directions of water flow. Lack of symmetry may also create transverse translational motion and a three dimensional trajectory. It seems reasonable to expect that the equations of rotation and translation would be largely uncoupled, at least to a first approximation. Without going into a detailed analysis, the author suspects that the primary effect of obstacle rotations would be to cause the form factors appearing in Equations (48) and (49) to vary with time. Since these are scale independent, the motion of the rotating and translating obstacle will likely also be invariant under scale changes. This conjecture could best be tested with the use of Wardlaw's hydrocode-coupled rigid body code, which allows six degrees of freedom.

Experimental Tests of the Shallow Explosion Scaling Theory

In the summer of 2005, field tests were conducted by SRI International, under the direction of P.Gefken, using 1/12-scale tetrahedron obstacles and a water depth of six inches.[14] Comp B charges weighing 7.3 grams and 28 grams were prepared that modeled the Mk 82 and Mk 84 bombs, respectively, and were configured in a manner consistent with the theory and calculations discussed above. Six replicated shots were conducted for both the Mk 82 scaled conditions and the Mk 84 scaled conditions. For both cases, all tetrahedrons in three of the shots were placed in a "toward" orientation and in an "away" orientation in the other three shots. A toward orientation means that the ground triangle (the side of the tetrahedron in contact with the ground) pointed symmetrically in the direction of the charge. The ground triangle pointed away from the charge for the away oriented tetrahedrons. The displacements of 54 tetrahedron obstacles were measured for each case.

Figure 10 shows the radial displacements of the obstacles in the 7.3-gram tests as a function of their initial radial standoffs (measured to the point on the ground below the top vertex). Diamond symbols denote the toward orientations and square symbols denote the away orientations. Different colors are used to identify different shots. The black solid line is the mean obstacle displacement from a regression fit to the scaled down full-scale Mk 82 test data, which are displayed here as small red plus symbols. The two dashed lines represent $\pm 2\sigma$ curves for the full-scale displacements. In the analysis of the full-scale data, the standard deviations were assumed to be proportional to the mean. This assumption is not fully realistic, but it is in reasonable agreement with the full-scale data. According to theory, about 98 percent of the displacement points should fall between the dashed lines. The full-scale analysis was based on the displacements of a total of 16 tetrahedron obstacles in four Mk 82 bomb tests.

Figure 10 suggests that the SRI radial displacement data agree reasonably well with the scaled down full-scale displacements. At 7 inches, the SRI data lie somewhat above the full-scale mean, while at 12 and 15 inches they appear to fall below the mean curve. The continuing upward trend shown by the SRI displacements at close-in initial standoffs is probably realistic, since the downturn of the full-scale mean is based upon only two data points. In theory, one would expect a downturn at some point as the initial standoff is reduced to zero. However,

in reality, the obstacle may break up before this is observed. The small-scale displacements appear to fall off more sharply with initial standoff than the full-scale data. The scatter of the SRI data looks much like the full-scale scatter, although there may be a local increase around 15 inches. There is no detectable difference between the displacements of obstacles with toward and away orientations.

Clearly the assumption that the standard deviation is proportional to the mean is incorrect since there is appreciable spread in the data after the mean has reached zero. A more correct assumption may be that the standard deviation is proportional to the mean of the total distance traveled. Calculations made by Wardlaw with a rigid body code for obstacle motions coupled to his Gemini hydrocode show that the obstacles move back and forth with the flow to a considerable extent before coming to rest.[11] This apparently produces the scatter at the larger distances. Although direct observation of the total travel distance would probably be difficult for each obstacle tested, suitable information could probably be obtained from Wardlaw's codes to revise the statistical analysis.

The angular displacements for the 7.3-gram shots, shown in Figure 11, suggest increased scatter for obstacles placed at the 18- and 21-inch standoffs. This could also reflect a dependence on the total travel distance. There does not appear to be an effect due to obstacle orientations, but more tests would be required to detect such differences.

A possibly significant difference between the full-scale and 1/12th-scale conditions is that the masses of the tetrahedrons in SRI's model tests appear to have been 10 to 20 percent low. The weight calculated for an idealized full-scale tetrahedron measuring 56 inches from

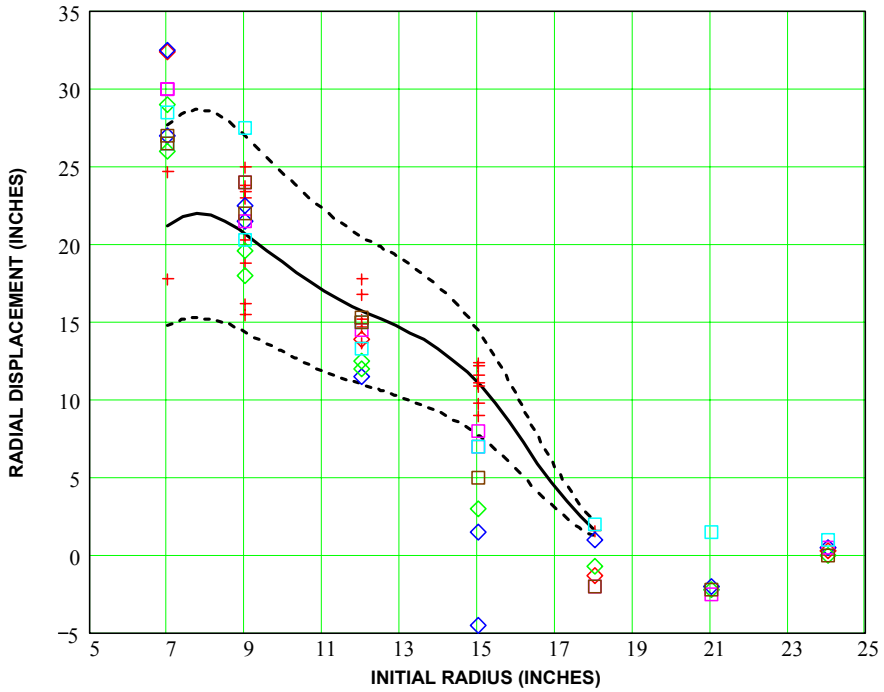

Figure 10. Comparison of 7.3-Gram Test Radial Displacements with Scaled Full- Scale Mean (Solid) and ±2σ Standard Deviation (Dashed) Curves. Colors Denote Different Shots. Diamonds and Squares Denote Toward and Away Orientations.

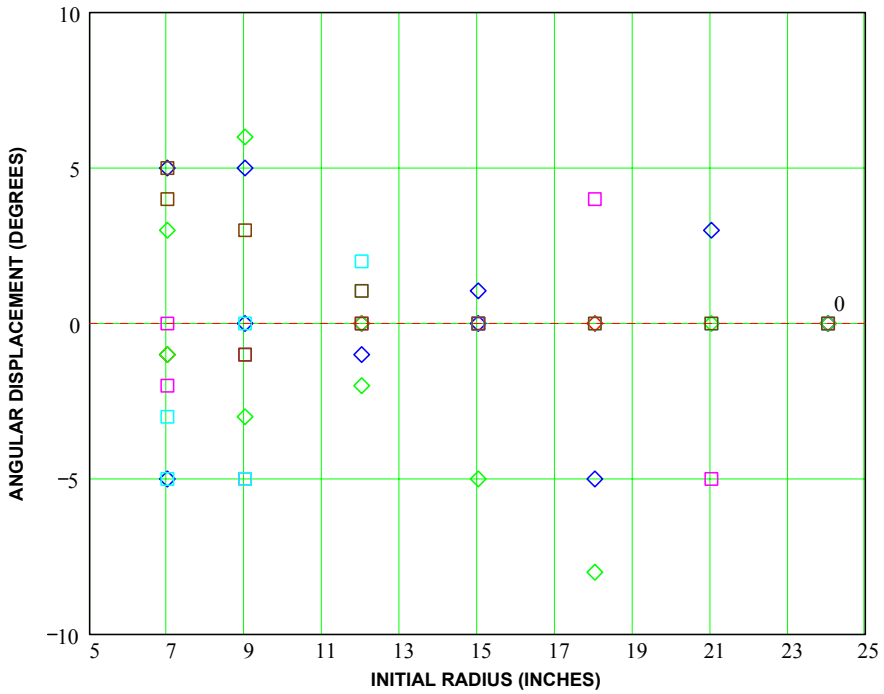

Figure 11. Angular Displacements in 7.3-Gram Tests. Colors Denote Different Shots. Diamonds and Squares Denote Toward and Away Orientations.

vertex to vertex, with a 5/8-inch thickness, leg widths of 4 inches in both directions, and using a steel density of 0.284 pounds per cubic inch, is 418 pounds. The density used corresponds to a linear weight of 15.7 lbs/ft for the angle steel. This result is somewhat lower than that estimated by Goeller and Rubin in Reference 13. At 1/12th-scale, the calculated tetrahedron mass would be 110 grams. The masses of the tetrahedrons used in the SRI tests were 93 ± 1 grams.[14] It is unclear how the lighter mass might have affected the results of the tests. Previous experiments conducted by SRI using 50-gram Comp B charges in water six feet deep and involving like obstacles of different masses showed that the heavier ones tended to become airborne more often than lighter obstacles.[15] It was thought by some participants in the effort that the additional inertia made it easier for the heavier obstacles to exit the water. It is reasonable to suspect that the lower inertias of the tetrahedrons may have resulted in premature stopping and perhaps a steepening of the slope of the mean curve.

Just prior to publication of this report it was learned[16] that the Mk 82 bombs used in the four full-scale tests had explosive weights that were about 9 percent below the standard weight of 192 lbs upon which the scaled tests were designed. It was also learned that the explosive used in the full-scale tests was H-6 instead of Tritonal, which had been assumed. Because the *J* value for H-6 is slightly below that of Tritonal (about 2 percent less), the full-scale displacements in Figure 10 represent a bomb with the same explosive and a weight that is, perhaps, 10 percent below the standard weight. This difference may account for the close-in disagreement between the model and full-scale displacements. It is reasonable to expect that displacement curve for the standard weight would be proportionately raised and the difference between the slopes of the full-scale and model-scale data lessened. The implications of this charge weight discrepancy will be further investigated in 2006.

The results for the 28-gram tests conducted by SRI are shown in Figures 12 and 13. No full-scale tests of the Mk 84 bomb in water six feet deep with obstacles have been conducted; hence, no full-scale comparisons can be made. The 28-gram test results again show, in both Figures 12 and 13, an increase in the scatter for the obstacles at intermediate distances from the charge. Qualitatively, the results are much like those of the 7.3-gram shots. An interesting detail seen in Figure 12, although not in Figure 10, is that the displacements of obstacles with toward orientations (diamonds) appear to be slightly higher than those with away orientations (squares) at close in positions. This might be expected from a theoretical viewpoint because the toward orientation, with two legs tilted toward the explosion, should generate more lift in the outflow direction and less in the inflow direction, thus favoring a greater net displacement.

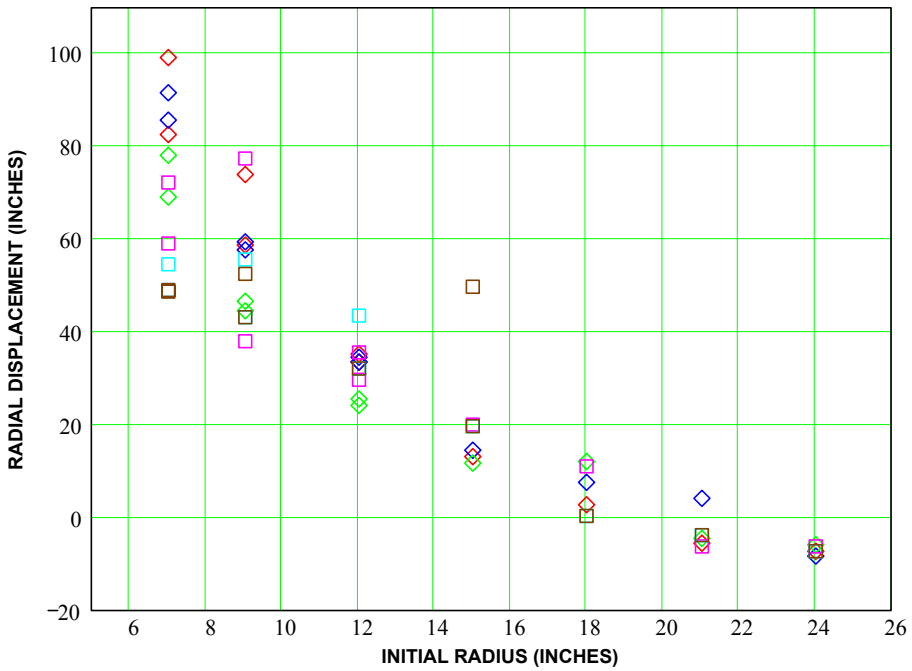

Figure 12. Radial Displacements in 28-Gram Tests. Colors Denote Different Shots. Diamonds and Squares Denote Toward and Away Orientations.

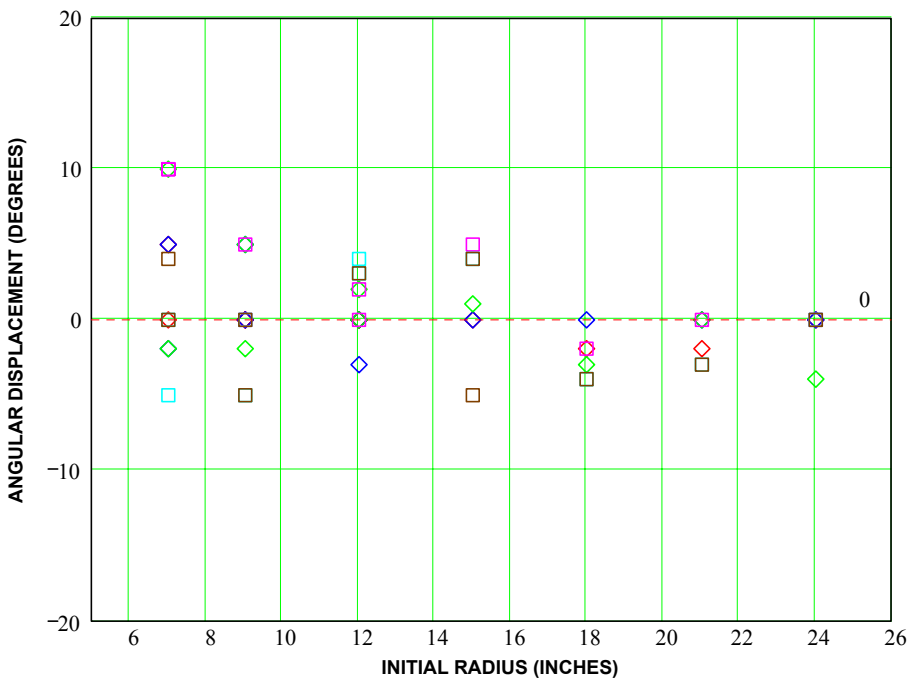

Figure 13. Angular Displacements in 28-Gram Tests. Colors Denote Different Shots. Diamonds and Squares Denote Toward and Away Orientations.

Conclusions and Recommendations

1. It appears that obstacle motions produced by full-scale explosions can be accurately reproduced in small-scale experiments when venting of the explosion bubble occurs. Model charge conditions that bring about a matching of the model-scale and scaled down full-scale cavity width versus time curves appear to successfully reproduce all hydrodynamic details of the water flow as well as the displacements of scaled obstacles placed in the flow. This matching process can be achieved by using hydrocodes that model the explosion flow effects. The appropriate time scale factor is the square root of the length scale factor, which can be set arbitrarily for the model experiment. Conditions for this computer-guided Froude scaling are close to those used for low pressure scaling, but they do not require reduction of the atmospheric pressure. Hence, they are appropriate for tests conducted in the field.

2. While the discussion in this report has been focused on scaling the flow effects of a single explosive charge, it would appear that the method can be extended to the multiple-charge scenario. It is likely that sizing the various charges could be done on a one-at-a-time basis using the method summarized above, but this suggestion should be the subject of future research.

3. It is recommended that the relationship between obstacle displacement and obstacle mass be investigated computationally using Wardlaw's Gemini-coupled rigid body obstacle displacement code.

4. It is recommended that additional testing be performed by SRI International using obstacles with masses that closely match those of the scaled down full-scale obstacles for the purpose of validating the computer-guided scaling approach discussed in the report. It is recommended that the experimental study also explore other factors that might affect the shape of the mean displacement versus initial standoff curve, such as sand characteristics.

5. It is recommended that the scaling bubbles that vent during the second cycle of expansion be explored computationally.

6. It is recommended that theoretical studies be funded to rigorously establish the concept of computer-guided scaling of shallow explosions.

7. It is recommended that the comparison between the full-scale and model tests be reviewed and consideration given to additional small-scale tests designed using the actual full-scale test charge weights.

References

1. Snay, H., *Model Tests and Scaling*, NOLTR 63-257, DASA 1240-I(3), 1964, (Downgraded to Unclassified 11 Feb 1966).

2. Szymczak, W. G., "Simulations of Violent Free Surface Dynamics," Proceedings of the Naval Platform Technology Seminar 2001, Paper 16, NPTS2001, 10 May 2001.

3. Szymczak, W. G., and Solomon, J. M., *Computations and Experiments of Shallow Depth Explosion Plumes*, NSWCDD/TR-94/156, August 1966.

4. Goertner, J.F., Hendrickson, J.R., and Leamon, R.G., *Model Studies of the Behavior of Underwater Explosion Bubbles in Contact with a Rigid Bottom*, Naval Ordnance Laboratory Technical Report NOLTR 68-207, March 1969.

5. Cole, R. H., *Underwater Explosions*, Princeton University Press, 1965 Dover Edition, New York, 1948.

6. Friedman, B., "Theory of Underwater Explosion Bubbles," *Communications in Pure and Applied Mathematics*, Vol. 3, 1950, pp. 177-199.

7. Snay, H.G., and Christian, E.A., *Underwater Explosion Phenomena: The Parameters of a Non-Migrating Bubble Oscillating in an Incompressible Medium*, NAVORD 2437, February, 1952.

8. Personal communication with W. Szymczak, NRL, January 2004.

9. Personal communication with A. Wardlaw, IHDNSWC, May 2005.

10. Personal communication with A. Wardlaw , IHDNSWC, November 2005.

11. Personal communication with A. Wardlaw , IHDNSWC, December 2003.

12. Goeller, J. and Ruben, K., *Effectiveness of General Purpose Bombs Against Beach and Surf Zone Obstacles*, ATR Interim Report, December, 2001.

13. Pozrikidis, C., *Introduction to Theoretical and Computational Fluid Dynamics*, Oxford University Press, New York, 1996.

14. Personal communication with P. Gefken, SRI International, August 2005.

15. Gefken, P., "Low Mass 1/12-Scale Obstacle Motion for Mk 82 and Mk 84 Bombs," Presentation at IHDNSWC, Indian Head, MD, 27 Feb 2003.

16. Personal communication with J. Allen, Naval Coastal Systems Center, Panama City, FL, December, 2005

DISTRIBUTION

UNIVERSITY OF MARYLAND
ATTN LESLIE C TAYLOR
3181 GLENN L MARTIN HALL
COLLEGE PARK MD 20742 1

AEROSPACE ENGINEERING DEPARTMENT
ATTN WILLIAM L FOURNEY
UNIVERSITY OF MARYLAND
COLLEGE PARK MD 20742 1

SPRINGPOINTE EXECUTIVE CENTER
ATTN WILLIAM MCDONALD
15210 DINO DRIVE
BURTONSVILLE MD 20866-1172 5

NAVAL RESEARCH LAB
ATTN BILL SZYMCZAK CODE 7131
WASHINGTON DC 20375 1

SPRINGPOINTE EXECUTIVE CENTER
ATTN KATHY RUBIN
15210 DINO DRIVE
BURTONSVILLE MD 20866-1172 1

SPRINGPOINTE EXECUTIVE CENTER
ATTN JACK GOELLER
15210 DINO DRIVE
BURTONSVILLE MD 20866-1172 1

OFFICE OF NAVAL RESEARCH
ATTN BRIAN ALMQUIST (321OE) RM 1091
ONE LIBERTY CENTER
875 NORTH RANDOLPH STREET SUITE 1425
OCEAN ENGINEERING & MARINE SYSTEMS
ARLINGTON VA 22203-1995 2

OFFICE OF NAVAL RESEARCH
ATTN TOM SWEAN (321OE) RM 1091
ONE LIBERTY CENTER
875 NORTH RANDOLPH STREET, SUITE 1425
OCEAN ENGINEERING & MARINE SYSTEMS
ARLINGTON VA 22203-1995 1

SRI INTERNATIONAL
ATTN PAUL GEFKEN
333 RAVENSWOOD AVE
MENLO PARK CA 94025 1

COMMANDING OFFICER
NSWC PANAMA CITY
ATTN CODE HS15 KENNARD WATSON
110 VERNON AVENUE
PANAMA CITY FL 32407-7001 1

COMMANDING OFFICER
NSWC PANAMA CITY
ATTN CODE HA11 JOHN ALLEN
110 VERNON AVENUE
PANAMA CITY FL 32407-7001 1

COMMANDING OFFICER
NSWC PANAMA CITY
ATTN CODE HS12 ANNE DAVENPORT
110 VERNON AVENUE
PANAMA CITY FL 32407-7001 1

NAVAL SURFACE WARFARE CENTER
ATTN RAY LEMAR
CODE E311 BUILDING 841
101 STRAUSS AVE
INDIAN HEAD MD 20640-5035 1

Electronic Copy:

ADMINISTRATOR
DEFENSE TECH INFORMATION CTR
ATTN JACK RIKE OCA
8725 JOHN J KINGMAN RD STE 0944
FT BELVOIR VA 22060-6218

Intenal:

C41 (TECHNICAL LIBRARY)	3
E123 (TOM KIDWELL)	2
E311 (AMOS DARE BLDG 301)	1
E311 (SEAN TIDWELL BLDG 841)	1
E311D (TONY KEE)	1
E311P (ANDREW WARDLAW)	10
E314 (TIM HENNESSEY)	1

This page intentionally left blank.

This page intentionally left blank.